HHS Public Access

Author manuscript

Nat Nanotechnol. Author manuscript; available in PMC 2019 July 21.

Published in final edited form as:

Nat Nanotechnol. 2019 March ; 14(3): 269–278. doi:10.1038/s41565-018-0342-5.

Endosomolytic Polymersomes Increase the Activity of Cyclic Dinucleotide STING Agonists to Enhance Cancer Immunotherapy

Daniel Shae[1], **Kyle W. Becker**[1], **Plamen Christov**[2], **Dong Soo Yun**[3], **Abigail K.R. Lytton-Jean**[3], **Sema Sevimli**[1], **Manuel Ascano**[4,5], **Mark Kelley**[7,8], **Douglas B. Johnson**[8,9], **Justin M. Balko**[4,6,8,9], and **John T. Wilson**[1,2,8,10,11,12,13,*]

[1]Department of Chemical and Biomolecular Engineering, Vanderbilt University, Nashville, TN, 37232

[2]Vanderbilt Institute of Chemical Biology, Vanderbilt University, Nashville, TN, 37232

[3]The David H. Koch Institute for Integrative Cancer Research, Massachusetts Institute of Technology, 77 Massachusetts Avenue, Cambridge, MA, 02139

[4]Department of Pathology, Microbiology and Immunology, Vanderbilt University Medical Center, Nashville, TN 37232

[5]Department of Biochemistry, Vanderbilt University Medical Center, Nashville, TN 37232

[6]Breast Cancer Research Program, Vanderbilt University Medical Center, Nashville, TN 37232

[7]Department of Surgery, Vanderbilt University Medical Center, Nashville, TN 37232

[8]Vanderbilt Ingram Cancer Center, Nashville, TN, 37232

[9]Department of Medicine, Vanderbilt University Medical Center, Nashville, TN 37232

[10]Department of Biomedical Engineering, Vanderbilt University, Nashville, TN, 37232

[11]Vanderbilt Center for Immunobiology, Vanderbilt University Medical Center, Nashville, TN 37232

[12]Vanderbilt Institute for Infection, Immunology, and Inflammation, Vanderbilt University Medical Center, Nashville, TN 37232

[*]**To whom correspondence should be addressed:** John T. Wilson, Ph.D., 2400 Highland Avenue, 107 Olin Hall, Nashville, TN 37212, **Phone:** +1-615-322-6406, john.t.wilson@vanderbilt.edu.

Author Contributions

D.S. and J.T.W. conceived of and designed the experiments. D.S. performed the majority of the experiments and data analysis. K.W.B. created the ISRE responsive luciferase reporter B16.F10 cells used for longitudinal *in vivo* experimentation and assisted with tumour therapy studies. P.C. synthesized and characterized 2'3-cGAMP. D.S.Y and A.K.R.L obtained cryo-transmission electron micrographs of nanoparticles. S.S. synthesized and characterized the pyridyl disulfide ethyl methacrylate monomer. M.A. assisted with experimental design and cGAMP characterization. M.K. and D.B.J provided resected tumour samples from melanoma patients. J.M.B. provided guidance on and assisted with nanoString experiments and analysis of multiplexed gene expression data. D.S. and J.T.W. wrote the manuscript.

Statistical Analysis. All statistical analyses were performed by using GraphPad Prism software, version 7.0.

Data Availability. The data that support the findings of this study are available from the corresponding author upon reasonable request.

[13]Vanderbilt Institute of Nanoscale Science and Engineering, Vanderbilt University, Nashville, TN 37232

Abstract

Cyclic dinucleotide (CDN) agonists of stimulator of interferon genes (STING) are a promising class of immunotherapeutic that activate innate immunity to increase tumor immunogenicity. However, the efficacy of CDNs is limited by drug delivery barriers, including poor cellular targeting, rapid clearance, and inefficient transport to the cytosol where STING is localized. Here we describe STING-activating nanoparticles (STING-NPs), rationally designed polymersomes for enhanced cytosolic delivery of the endogenous CDN ligand for STING, 2'3' cyclic guanosine monophosphate-adenosine monophosphate (cGAMP). STING-NPs increase the biological potency of cGAMP, enhance STING signaling in the tumour microenvironment and sentinel lymph node, and convert immunosuppressive tumours to immunogenic, tumouricidal microenvironments. This leads to enhanced therapeutic efficacy of cGAMP, inhibition of tumour growth, increased rates of long-term survival, improved response to immune checkpoint blockade, and induction of immunological memory that protects against tumour rechallenge. We validate STING-NPs in freshly isolated human melanoma tissue, highlighting their potential to improve clinical outcomes of immunotherapy.

Immune checkpoint blockade (ICB) is revolutionizing the treatment of a diversity of cancers and can yield complete and durable responses.[1,2] These remarkable outcomes provide evidence that the immune system can be harnessed to combat metastatic disease. However, patients often do not respond to FDA approved ICB antibodies,[1–3] invigorating a fervor of investigation into strategies to increase the number of patients that will benefit from immunotherapy.[4,5] For many tumour types, patient survival and response to ICB correlates with an immunogenic ("hot") tumour microenvironment (TME) infiltrated with tumour antigen-specific T cells, primarily $CD8^+$ T cells, that are reactivated in response to checkpoint blockade antibodies.[6–8] However, many patients have immunologically "cold" tumours that lack significant T cell infiltration and are instead characterized by high densities of immunosuppressive cells that inhibit antitumour immunity. This has motivated the need for strategies to reprogram "cold" tumours towards immunogenic, pro-inflammatory states that reinvigorate antitumour T cell responses.

Stimulator of interferon genes (STING) is a cytosolic pattern recognition receptor that is critical for spontaneous induction of antitumour T-cell immunity.[9,10] The STING pathway is activated in response to tumour-derived DNA in the cytoplasm, which is detected by the enzyme cyclic-GMP-AMP synthase,[11–14] leading to the production of 2',5–3'5' cyclic guanosine monophosphate-adenosine monophosphate (cGAMP), the endogenous and high affinity ligand for STING.[15,16] Activation of STING triggers a multifaceted type I interferon (IFN-I) driven inflammatory program that stimulates dendritic cell (DC) activation and cross-presentation of tumour antigen for the subsequent priming of antitumour T cells.[17] Accordingly, STING-deficient mice have a higher susceptibility to tumour formation, diminished antitumour T cell immunity, and impaired responses to immunotherapy.[9,18,19] The critical role of STING in cancer immune surveillance has motivated recent investigations leveraging cGAMP and structurally-related cyclic dinucleotide (CDN) STING

agonists as therapeutics to stimulate antitumour immunity.[20–24] While promising, the activity and therapeutic efficacy of exogenously delivered cGAMP – an anionic, highly water-soluble molecule – is limited by its low bioavailability and poor drug-like properties. As a result, cGAMP does not readily cross the cellular plasma membrane, is poorly endocytosed, and, critically, has limited access to the cytosol where STING is located.[25,26] Moreover, CDNs are rapidly cleared with modest delivery to tumours and/or lymphoid organs.[27,28]

The activity of CDNs is further limited by a lack of drug carriers optimized for this unique class of compound.[29] Here, we address the challenges limiting the therapeutic impact of CDNs through the design of a STING-activating nanoparticle (STING-NP) based on polymer vesicles (polymersomes) engineered for efficient cytosolic delivery of cGAMP (Figure 1a,b). Through control of polymer properties, formulation methodologies, and an *in situ* vesicle membrane crosslinking strategy, cGAMP is efficiently encapsulated into polymersomes that disassemble in response to endolysosomal acidification to unveil membrane-destabilizing polymer segments that promote endosomal escape of cGAMP. Consequently, STING-NPs enhance the biological activity of cGAMP by 2–3 orders of magnitude in multiple immunologically relevant cell types and trigger an IFN-I-driven innate immune response that induces a shift to a “hot” T cell-inflamed TME. STING-NPs increase the therapeutic efficacy of cGAMP and improve responses to ICB in a poorly immunogenic murine melanoma model when administered via either an intratumoural or intravenous route. Moreover we validate activity of STING-NPs in resected human metastatic melanoma tissue, demonstrating the translational potential of STING-NPs as a platform for increasing tumour immunogenicity.

Results and Discussion

Design of endosomolytic polymersomes for cytosolic delivery of cGAMP

To optimize STING-NPs for cGAMP delivery, we designed polymersomes with an aqueous core for efficient hydrophilic drug loading and a vesicle membrane comprising amphiphilic diblock copolymer chains with pH-responsive, membrane destabilizing activity to mediate intracellular release and endosomal escape of cGAMP (Figure 1a,b). We synthesized well-defined poly(ethylene glycol)-*block*-[(2-diethylaminoethyl methacrylate)-*co*-(butyl methacrylate)-*co*-(pyridyl disulfide ethyl methacrylate)] (PEG-DBP) copolymers using reversible addition-fragmentation chain transfer polymerization. pH-sensitive, cationic 2-(diethylamino)ethyl methacryate (DEAEMA) groups and hydrophobic butyl methacrylate (BMA) moieties were integrated at a molar ratio previously reported to be optimal for endosomal escape.[30,31] Thiol-reactive pyridyl disulfide ethyl methacrylate (PDSMA) groups were copolymerized into the second block for *in situ* crosslinking of chains within the vesicle membrane via partial reduction with dithiothreitol (DTT). To achieve high encapsulation efficiencies, polymersomes were formulated via a modified direct hydration method[32] that enables a high volume ratio of polymer to encapsulant during the vesicle assembly process.

The resulting particles were PEGylated, surface neutral vesicles with a median hydrodynamic diameter of ~80 nm at pH 7.4 (Figure 1c-e). Polymerization conditions were

chosen to incorporate an average of ~2 PDSMA groups per chain to prevent the formation of a fully crosslinked network structure within polymersomes. Polymersomes therefore retained pH-responsive disassembly after crosslinking, as demonstrated by a decrease in nanoparticle diameter at endosomal pH (Figure 1f). Chain crosslinking was observed directly via an increase in molecular weight (M_n=11kDa; PDI=1.2) (Figure 1g) and the release of 2-pyridinethione (Supplementary Figure S1a). No evidence of interparticle crosslinking was observed in dynamic light scattering analysis of particles before and after crosslinking (Supplementary Figure S1b–d).

We next evaluated the pH-responsive, membrane destabilizing activity of polymersomes using an erythrocyte haemolysis assay that is commonly used to predict endosomolytic activity of drug carriers.[33,34] Vesicle membrane crosslinking enhanced haemolytic activity at endosomal pH relative to uncrosslinked variants, likely due to an increased average molecular weight of membrane destabilizing DBP polymer blocks upon crosslinking (Figure 1g). This is consistent with findings that pH-dependent haemolytic activity of PEG-*bl*-[DEAEMA-*co*-BMA] (PEG-DB) polymers correlates positively with increasing molecular weight of the DB block (Figure 1i). While weakly haemolytic PEG_{2k}-DB_{5kDa} and PEG_{2kDa}-$DBP_{4.5kDa}$ polymers self-assembled into polymersomes that encapsulated cGAMP, all larger PEG_{2kDa}-$DB_{8–36kDa}$ polymers formed poorly-defined, colloidally unstable aggregates (Supplementary Table S1), consistent with a weight fraction of PEG less than 0.25 for which vesicle assembly is not expected.[35] To determine if haemolytic activity could be increased while maintaining a vesicular structure, we synthesized PEG-DB with larger (5 and 10kDa) PEG blocks. However, these polymers assembled into worm-like or spherical micelles (Supplementary Figure S2), likely driven by increased steric repulsion in polymer chains with long PEG coronas, a well-documented effect that disfavors vesicular self-assembly due to the relatively low surface curvature of bilayer structures.[36,37] Without aqueous cores, micellar morphologies demonstrated lower cGAMP loading than PEG_{2kDa}-DBP_{5kDa} vesicles. These results revealed an inherent tension between achieving potent haemolytic activity and the assembly of cGAMP-loaded, PEG-DB vesicles, and motivated the use of low molecular weight PEG_{2kDa}-$DBP_{4.5kDa}$ chains in conjunction with *in situ* vesicle crosslinking in the design of STING-NPs.

STING-NPs Increase the Immunostimulatory Potency of 2’3’-cGAMP

Given the critical role of IFN-I in antitumour immunity,[38] we evaluated the ability of STING-NPs to stimulate IFN-I responses in monocyte, macrophage, and melanoma cell lines (Figure 1j). Delivery of cGAMP in crosslinked PEG-DBP vesicles increased cGAMP activity by several orders of magnitude (EC_{50} = 67±12 nM, 36±14 nM, and 230±1.0 nM in THP-1 ISG, RAW ISG, and B16 ISG cell lines, respectively), whereas free cGAMP elicited little response even at high concentrations (EC_{50} = 31±1 μM, 22±4 μM, 55±2 μM). A similar enhancement in cGAMP potency was observed in both DC2.4 DCs and bone marrow derived DCs (Supplementary Figure S3). We observed a relationship between haemolytic activity at endosomal pH values and increased STING-NP activity, as weakly haemolytic PEG-DB and uncrosslinked PEG-DBP vesicles only modestly increased cGAMP activity.

Mixing cGAMP with pre-formulated vesicles resulted in a negligible increase in activity, indicating that cGAMP encapsulation was critical to efficient STING activation. This finding was further supported by evaluating the activity of PEG-DB polymers that did not form vesicular structures. Although we observed some association between cGAMP and the micellar structures formed using higher molecular weight PEG-DB polymers, we found that these morphologies mediated minimal enhancements in cGAMP activity despite being highly haemolytic (Supplementary Figure S4). This highlights an important distinction between delivery of oligonucleotide therapeutics (e.g., siRNA), which can be stably complexed to cationic carriers via a multivalent electrostatic interaction,[39] and CDNs, which may lack a sufficient degree of charge for stable electrostatic complexation with DEAEMA groups.

We next evaluated the capacity of polymersomes to enhance cellular uptake of cGAMP by co-encapsulating cGAMP with a fluorescently labeled CDN (cdGMP-Dy547). While cdGMP-Dy547 uptake varied between cell types, STING-NPs increased uptake ~1.5–3.5x, with no significant differences observed between crosslinked and uncrosslinked STING-NPs (Figure 1k). While some increase in cGAMP activity can be attributed to enhanced intracellular uptake, the magnitude of reduction in EC_{50} achieved with STING-NPs is likely primarily a consequence of enhanced endosomal escape and cytosolic delivery of cGAMP. Hence, by combining precisely designed diblock copolymers, a formulation method that enables high cGAMP encapsulation efficiency (~38%), and vesicle membrane crosslinking to enhance endosomolytic activity, STING-NPs enhance cGAMP potency 240–610 fold, the largest carrier-mediated fold-increase in CDN activity reported to date.[26,40]

Next, subcutaneous B16.F10 melanoma tumours (~100 mm^3) grown in immunocompetent mice were treated via intratumoural injection with STING-NP, free cGAMP, or vehicle (PBS) and harvested 4h later for qPCR gene expression analysis. Compared to free cGAMP and vehicle, STING-NPs increased expression of interferon-β1 (*Ifnb1;* 6.3-fold over free cGAMP), *Cxcl9* (6.6 fold) and *Cxcl10* (4.9 fold; Figure 2a), critical mediators of antitumor T cell activation and recruitment.[17,41] Similar to previous reports,[21] *Ifnb1* expression was highly variable at 4h, likely due to tumour heterogeneity and tight temporal regulation of gene expression levels. Nonetheless, there was a positive linear correlation between *Ifnb1* and *Cxcl9* and *Ifnb1* and *Cxcl10* levels in treated mice (Supplementary Figure S5), consistent with a STING-driven inflammatory response. Interferon-mediated inflammation was further monitored through longitudinal optical imaging using tumours expressing an Interferon Stimulated Response Element (ISRE) luciferase reporter. A single STING-NP treatment resulted in an elevated and extended interferon response in the tumour, while free cGAMP did not elicit a response above baseline (Figure 2b). Intratumoural administration of STING-NPs was well tolerated with mice exhibiting minimal, transient weight loss. Analysis of blood chemistry and liver histology revealed no evidence of liver or kidney toxicity caused by STING-NPs (Supplementary Figure S6).

We further characterized gene expression profiles using multiplexed gene expression analysis (nanoString; Figure 2c-e, Supplementary Figure S7). Of >700 genes, expression levels of *Il6* and *Ifnb1* were most significantly upregulated (~1000-fold) relative to vehicle controls, consistent with STING-mediated IRF3 and NF-κB signaling.[16] More generally,

STING-NPs triggered a multifaceted shift to an inflamed and tumouricidal microenvironment, with significant upregulation of interferon-stimulated genes, pro-inflammatory cytokines, leukocyte-recruiting chemokines, pro-apoptotic mediators, genes associated with DC maturation and T-cell priming, and markers of NK and T cell activation (Figure 2c). Several immunosuppressive mediators were also upregulated, which likely act as endogenous negative regulators of STING activation.[16] Some of these genes are the targets of pharmaceuticals that are either clinically advanced (e.g., PD-L1, IDO-1) or in development (e.g., IL-10, arginase 2) and are potential candidates for combination therapy with STING-NPs. While not explored herein, an attractive feature of STING-NPs is the ability to efficiently encapsulate a diversity of cargo, offering opportunities for co-delivery of CDNs with other intracellular-acting immunomodulators.

To elucidate differences between STING-NP and cGAMP treatment, the most differentially expressed genes were ranked by the fold-change expression level between STING-NP and cGAMP treated tumours (Figure 2d). In selected genes we observed a consistent 5–10-fold increase in gene expression in mice treated with STING-NP versus cGAMP, with the exception of *Cxcl1* (35-fold) and *Ifna2* (20-fold). Treatment with STING-NPs and free cGAMP elicited directionally similar changes in transcriptional profiles, suggesting a similar mechanism of action and minimal off target effects associated with STING-NPs. This was further corroborated by unsupervised hierarchal clustering of genes with significantly different expression levels relative to vehicle control, which revealed similar gene clusters between cGAMP and STING-NP treated tumours (Figure 2e).

B16.F10 melanoma tumours were injected with STING-NPs co-loaded with cGAMP and cdGMP-Dy547 or a mixture of soluble cGAMP and cdGMP-Dy547, and flow cytometry was used to quantify cellular uptake of cdGMP-Dy547 (Figure 2f,g). cdGMP-Dy547 was most commonly localized in DCs ($CD11c^+MHC\text{-}II^+$), natural killer (NK) cells ($CD45^+NK1.1^+$), and macrophages ($CD11b^+F4/80^+$), with STING-NPs increasing the degree of CDN uptake in NK cells, DCs, and $CD45^-$ cells, with less significant increases observed in macrophages ($CD11b^+F4/80^+$) and myeloid derived suppressor cells (MDSC) ($CD11b^+Gr\text{-}1^+$), and negligible uptake of both free and encapsulated CDN by T-cells ($CD3^+$). Amongst these cells, cdGMP-Dy547 uptake was highest in NK cells, DCs, and macrophages (Figure 2g). Cultured DCs (DC2.4), macrophages (RAW264.7), NK cells, and B16.F10 melanoma cells were incubated with STING-NPs and *Ifnb1* levels measured. Macrophages and DCs expressed the highest levels of *Ifnb1* in response to STING-NPs, whereas minimal expression was observed in B16.F10 tumour cells or NK cells (Figure 2h). Collectively, these data indicate that macrophages and DCs are the primary immunocellular targets of STING-NPs.

Lymph nodes act as command centers for orchestrating antitumour immunity, yet, like the tumour site, are often highly immunosuppressed, resulting in impaired priming of antitumour T cells.[42] Nanoparticles in the 20–100 nm range preferentially drain through the lymphatics after interstitial injection, resulting in enrichment of cargo within local draining lymph nodes.[27,43,44] Consistent with this phenomenon, STING-NPs increased cdGMP-Dy547 accumulation in the sentinel (inguinal) lymph node relative to free CDN, which was undetectable above background (Figure 2i). This was further supported by significant

elevation of *Ifnb1* expression in the inguinal lymph node post-administration of STING-NP relative to free cGAMP, which failed to stimulate IFN-I (Figure 2j). Therefore, in addition to their capacity for potent STING activation, another important advantage of STING-NPs – and a key distinction from small molecule STING agonists – is their ability to enhance CDN uptake and STING signaling in the sentinel LN.

STING-NPs stimulate an immunogenic, T cell-inflamed tumour microenvironment

We next evaluated the effect of STING-NPs on the immunocellular composition of the B16.F10 melanoma TME. A single intratumoural treatment with STING-NPs dramatically increased the number of tumour infiltrating $CD11b^+Ly6c^+Ly6g^+$ activated neutrophils[45] relative to free cGAMP(Figure 3a). This is consistent with the substantial increase in STING-NP treated tumours of the neutrophil chemokine *Cxcl1*.[46] Additionally, surface expression of CD206, a canonical marker of M2-polarizedmacrophages, was decreased on macrophages in STING-NP treated tumours (Figure 3b), suggesting repolarization or recruitment of macrophages with reduced immunosupressive capacity. DC expression of CD86 in the TDLN (Figure 3c) was also increased, consistent with enhanced CDN accumulation in LNs. Free cGAMP and STING-NPs promoted the influx of similar numbers of monocytic MDSCs with immunosupressive potential (Figure 3a), likely a regulatory response to restrict STING-mediated inflammation and a potential target for combination therapy.[47] STING-NPs also significantly increased the number of infiltrating $CD8^+$ and $CD4^+$ T cells (Figure 3d,e). Additionally, STING-NP treatment increased the $CD8^+/CD4^+$ T cell ratio, a commonly reported prognostic indicator of response to immunotherapy and clinical outcome.[48–50] *Ex vivo* PMA/ionomycin restimulation of T cells revealed that STING-NPs also significantly increased the percentage of IFN-γ and TNF-α secreting $CD4^+$ T cells and TNF-α^+CD8^+ T cells in the TME relative to cGAMP, indicating enhanced antitumour functionality of infiltrating T cells in STING-NP treated tumours (Figure 3g); no significant changes in the percentage of $CD4^+$ or $CD8^+$ T cells secreting the immunosuppressive cytokines IL-4 and IL-10 were observed (Supplementary Figure S8).

STING-NPs enhance the therapeutic efficacy of cGAMP

We first evaluated therapeutic efficacy using an intratumoural administration route explored clinically (Figure 4a-e).[51] Using a poorly immunogenic B16.F10 melanoma model, we initiated treatment in mice with established (~14 day) and relatively large (111 ± 16 mm^3) subcutaneous tumours, which are more challenging to treat with immunotherapy than are smaller tumours.[52,53] Treatment with STING-NPs resulted in an eleven-fold decrease in tumour growth rate (doubling time $(DT)_{STING\text{-}NP}$ ~ 22.7d) and significant increase in survival time relative to cGAMP, which resulted in only a modest suppression of tumour growth (DT_{cGAMP} ~ 3.5d, DT_{PBS} ~ 2.2d) that did not confer significant survival benefit (median survival $(MS)_{PBS}$ =11d, MS_{cGAMP} = 12d, $MS_{STING\text{-}NP}$ = 29d). Treatment with empty particles did not affect tumour growth. Importantly, a physical mixture of cGAMP with pre-formulated empty vesicles yielded a nearly identical response as cGAMP, further corroborating *in vitro* data demonstrating the importance of encapsulating cGAMP into vesicles for achieving potent STING activation.

Approximately one-third of mice treated intratumoural with STING-NPs completely rejected tumours, without evidence of residual burden up to 65 days after tumour inoculation (Figure 4e). We rechallenged these complete responders with B16.F10 tumour cells on the opposite flank and monitored tumour volume. Without any additional treatment, 5/7 (~70%) rechallenged mice completely resisted tumour growth through at least 150 days. Tumour growth in the remaining two mice was also significantly slower relative to age-matched, treatment-naïve controls (Figure 4f,g). To evaluate if intratumoural injection of STING-NPs could suppress distal tumour growth, two SC B16.F10 tumours were concurrently established on contralateral flanks, and one tumour was injected with STING-NP, cGAMP, or PBS (Figure 4h-j). STING-NP treatment significantly slowed the growth of the non-treated, contralateral tumour relative to PBS (DT_{PBS}, ~1.9d, $DT_{STING\text{-}NP}$ ~3.0d) though to a lesser extent than the treated tumour (DT_{PBS}~1.7d, $DT_{STING\text{-}NP}$ ~ 5.3d). Combining STING-NP treatment with systemic administration of anti-PD-1 and anti-CTLA-4 ICB further inhibited growth of the untreated contralateral tumour ($DT_{STING\text{-}}$NP+ICB ~ 5.9d). (Figure 4j). ICB, alone or in combination with free cGAMP, had no significant effect on growth of either tumour.

While localized intratumoural delivery of STING agonists and other immunomodulators is emerging as a clinically viable treatment modality, this administration route may not be feasible for many patients and/or cancer types, particularly in the setting of advanced, metastatic disease.[17] We therefore evaluated the therapeutic efficacy of STING-NPs administered systemically via an intravenous route (Figure 4k-o). Systemically administered STING-NP slowed subcutaneous tumour growth relative to free cGAMP, which demonstrated no therapeutic benefit (DT_{PBS} ~ 1.9d, DT_{cGAMP} ~ 1.9d, $DT_{STING\text{-}NP}$ ~3.8d) even when combined with ICB ($DT_{cGAMP+ICB}$ ~ 2.8d). By contrast, systemic STING-NP significantly improved response to anti-PD-1 + anti-CTLA-4 ICB ($DT_{STING\text{-}NP+ICB}$ ~ 5.0d). Improved responses to ICB were not observed using a mixture of empty NPs and free cGAMP. A mild acute decrease in body weight was observed following IV administration of STING-NPs, followed by full weight recovery without elevation in serum levels of ALT, bilirubin, or creatinine over mice administered PBS; additionally, histological analysis revealed no evidence of liver damage due to administration of STING-NPs (Supplementary Figure S9). Importantly, 40% (4/10) of mice administered STING-NPs systemically in combination with ICB exhibited complete responses, with no evidence of tumour burden for at least 55 days after cessation of therapy (Figure 4o). This is the first demonstration that intravenously administered CDN STING agonists can confer significant survival benefit while synergizing with ICB to yield complete and durable responses, offering an opportunity to utilize STING agonists in patients with non-accessible tumours.

To support the translational potential of STING-NPs, we directly injected freshly resected human metastatic melanoma tissue specimens with STING-NP, cGAMP, or PBS, and quantified *Ifnb1*, *Tnfa, and Cxcl10* levels via qPCR (Figure 5). Consistent with findings in murine models, STING-NPs demonstrated superior immunostimulatory activity, increasing expression of *Ifnb1* (48–352 fold) and *Tnf* (4–5 fold) as well as *Cxcl10* (15–23 fold), a chemokine that correlates with T cell infiltration in human metastatic melanoma.[41] This effect was consistent in tumours from two different melanoma patients, supporting the

potential use of STING-NPs as a strategy to increase the immunogenicity of human tumours.

Conclusions

Through rational design of nanoparticle properties, we have designed endosomolytic polymersomes to enhance the cytosolic delivery of cGAMP. Owing to both their nanoscale properties and immunostimulatory activity, STING-NPs provide advantages over existing STING agonists and CDN delivery technologies in terms of 1) superior activation of the STING pathway; 2) ability to activate STING in both the tumour and sentinel lymph node; 3) therapeutic efficacy achieved through both intravenous and intratumoural administration routes, and 4) enhanced synergy with immune checkpoint blockade. In doing so, this work also elucidated important relationships between polymer structure, colloidal self-assembly, and CDN delivery, highlighting key distinctions between delivery of nucleic acid therapeutics and CDNs while establishing new design principles for nanoparticle delivery of STING agonists. Our findings indicate that STING-NPs enhance cytosolic delivery of cGAMP via an endosomal escape mechanism, preferentially activating STING in myeloid cell populations within the TME and TDLN to trigger a multifaceted shift to a “hot” T cell-inflamed TME that inhibits tumour growth. As a single agent, locally administered STING-NPs can generate robust and complete responses, eliciting systemic antitumour immunity that can protect against tumour rechallenge. Importantly, STING-NPs can be administered through both intratumoural and intravenous routes either as monotherapy or in combination with ICB for therapeutic benefit, potentially opening new clinical opportunities for leveraging STING agonists. Therefore, STING-NPs represent a significant technological advancement with potential to expand the immunotherapeutic armamentarium.

Methods

Synthesis and Characterization of Block Copolymers.

Butyl methacrylate (BMA), poly(ethylene glycol) 4-cyano-4-(phenylcarbonothioylthio)pentanoate, M_n=2,000 Da and M_n=10,000 Da (PEG-CPADB), 4-cyano-4-(phenylcarbonothioylthio)pentanoate (CPADB), N,N’-Dicyclohexylcarbodiimide (DCC), 4-(Dimethylamino)pyridine (DMAP), DL-Dithiothreitol (DTT), 4,4’-azobis(4-Cyanovaleric acid) (V501), dichloromethane, 1,4-dioxane, and poly(ethylene glycol) methyl ether (M_n = 5,000 Da) were purchased from Sigma-Aldrich. 2-(Diethylamino)ethyl methacrlate (DEAEMA) was procured from TCI Chemicals, and 2,2’-Azobis(4-methoxy-2,4-dimethylvaleronitrile) (V70) was purchased from Wako Chemicals. Pyridyl disulfide ethyl methacrylate (PDSMA) was synthesized according to a previously reported procedure.[54] BHT inhibitor was removed from methacrylate monomers before further use by gravity chromatography using basic alumina (Sigma).

For synthesis of PEG-b-DB polymers, the appropriate PEG-CPADB macroRAFT chain transfer agent (mCTA) was dissolved in anhydrous dioxane with purified BMA, DEAEMA, and V501 at a 60:40 molar ratio of BMA:DEAEMA, sealed with septa, purged with N_2 for 20 minutes, and polymerized at 70˚C for 18 h. An initiator to mCTA (I:mCTA) ratio of 0.2:1 was used with a combined monomer and mCTA to dioxane weight ratio of 0.4. Polymers

were precipitated 2x in cold pentane and vacuum dried. Polymer composition were characterized via ^{1}H-NMR in $CDCl_3$ on a Bruker AV400 spectrometer (Supplementary Figure S10). Molecular weight and polydispersity index (PDI) were quantified using gel permeation chromatography (Agilent) with DMF containing 0.1M LiBr as the mobile phase and in line light scattering (Wyatt) and refractive index (Agilent) detectors. PEG_{5kDa}-CPADB or PEG_{10kDa}-CPADB mCTAs were synthesized as previously described.[55] PEG_{2kDa}-$DBP_{4.5kDa}$ was synthesized with similar conditions, substituting V70 for V501 and a reaction temperature of 30°C for 24h.

Synthesis of 2'3'-cGAMP.

2'3'-cGAMP was synthesized using a method adapted from Gaffney *et al* (Scheme S1).[56] Adenosine phosphoramidite, (1 g, 1 mmol) was dissolved in 7 ml of acetonitrile (ACN) and water (0.036 mL, 2 mmol). Pyridinium trifluoroacetate (0.231 g, 1.2 mmol) was added and the reaction mixture was stirred for 1 min. tert-Butylamine (8 ml) was added and the reaction mixture was stirred for 10 min at room temperature. Solvent was removed by rotary evaporation to yield a gummy residue that was dissolved in 15 ml of dichoromethane (DCM). Sequentially, water (0.18 ml, 10 mmol,) and dichloroacetic acid (DCA, 27 ml, 3% in DCM, 10 mmol) were added and the reaction mixture was stirred at room temperature for 10 min. Pyridine (1.6 ml, 20 mmol) was added and solvent was removed by rotary evaporation. The residue was dissolved in 10 ml of ACN and concentrated. This process was repeated three times. The oily product was dissolved in anhydrous ACN (3 mL) and a solution of guanosine phosphoramidite (1.27 g, 1.2 mmol, dissolved in 3 mL of anhydrous ACN) was added. The guanosine phosphoramidite was co-evaporated with anhydrous ACN (3 × 20 mL) and vacuum dried overnight. After stirring for 2 min, anhydrous tert-Butyl hydroperoxide (5.5 M in decane, 0.55 ml, 3 mmol) was added and the reaction mixture was additionally stirred for 30 min at room temperature. $NaHSO_3$ (0.3 gr, dissolved in 0.8 ml H2O) was added and the mixture was stirred for 5 min. Solvent was removed by rotary evaporation. The oily product was dissolved in DCM (18 mL), and water (0.18 ml, 10 mmol) and dichloroacetic acid (DCA, 27 ml, 3% in DCM, 10 mmol). The reaction mixture was stirred for 10 min at room temperature and quenched with pyridine (10 mL). Solvent was removed by rotary evaporation and the residue was co-evaporated with anhydrous pyridine (2 ×10 mL). The oily residue was dissolved in anhydrous pyridine (17 mL) and 5,5-dimethyl-2-oxo-2-chloro-1,3,2-dioxaphosphinane (0.65 g, 3.5 mmol) was added. The reaction mixture was stirred at room temperature for 10 min and then water (0.63 mL, 35 mmol) and iodine (0.330 g, 1.3 mmol) were added sequentially. After stirring for 5 min, the reaction mixture was poured into solution of $NaHSO_3$ (0.2 gr, in 150 mL of water). Solid $NaHCO_3$ (4g) was slowly added after 5 min and the stirring was continued for 5 min. The water was transferred into a separatory funnel and a mixture of ethyl acetate and diethyl ether was added (150 ml, 1:1). The organic layer was separated and the aqueous layer was extracted with an additional mixture of ethyl acetate and diethyl ether (80 ml, 1:1). The organic layers were combined and concentrated to an oil. The residue was purified by flash chromatography (Combi-flash Rf, DCM/methanol = 0–25% for 20 min) to give a solid. The solid was dissolved in CH_3NH_2 in anhydrous EtOH (33% by weight, 24 ml, 212 mmol). The reaction mixture was stirred at room temperature for 4 hr. The solvent was removed by rotary evaporation to give a solid. The solid was co-evaporated with a mixture of anhydrous

pyridine and triethyl amine (4 times, 5 ml, 4:1) to give an oily product. The oily product was dissolved in anhydrous pyridine (2 mL) and triethyl amine (8 ml) and Et3Nx3HF (3.3 ml, 60 mmol F-, 30 eq. rel to each TBS) were added simultaneously. The reaction mixture was stirred at 55°C for 3h. After the reaction mixture was cooled down, acetone (HPLC grade, 80 ml) was slowly added. The precipitate was filtered off and washed with acetone (5 × 5 ml). The final compound was purified on a Gemini–NX C18 column (250 mm × 10 mm, flow rate 5 mL/min with UV detection at 254 nm) using a gradient of 1 to 5% for 20 min (CH_3CN in 0.1 M NH_4HCO_3). ^{1}H-NMR spectra (Supplementary Figure S11) and LC-MS data (Supplementary Figure S12) of purified 2'3'-cGAMP are provided in the Supplementary Information. The biological activity of synthesized 2'3'-cGAMP, both free and incorporated into STING-NPs, was validated by comparison to a commercial source (2'3-cGAMP VacciGrade™, Invivogen: Supplementary Figure S13).

Polymer self-assembly and particle characterization.

Block copolymers were mixed with ethanol to a concentration of 1250 mg/mL and allowed to equilibrate for at least 20 minutes in a 2 mL microfuge tube at 37˚C. 1x volume equivalent of DI H_2O containing the encapsulant (50 mg/mL cGAMP) was added to the polymer mixture, followed by centrifugation at 2000xg for 2 minutes. The mixture was allowed to equilibrate for 20 minutes before 3x volume of 25% EtOH in H_2O was added to the mixture and centrifuged again for 2 minutes. 7.5x volume equivalents of H_2O was added to the mixture, which was briefly vortexed and sonicated at 40˚C until the polymer was completely dispersed into colloidal suspension. For crosslinked PEG-b-DBP particles, the particle suspension was diluted to 1 mL and crosslinked through addition of aqueous DTT. To purify and concentrate the particles, the sample was diluted to 15 mL in DI H_2O followed by centrifugal dialysis, twice (Amicon, 10kDa MWCO). For cGAMP loaded particles, an aliquot was removed, added to 9 volumes of pH 5.8 PBS, and analyzed by HPLC with an isocratic mobile phase of H_2O with 0.1% trifluoroacetic acid to determine cGAMP concentration.

To measure particle size distribution and zeta potential, particles were diluted into 10 mM PBS of the appropriate pH and characterized using a Malvern Nano ZS. For transmission electron microscopy, particles were drop cast onto an ultrathin carbon / lacey support grid (TedPella), stained with a 2% solution of methylamine tungstate for 30 seconds, and imaged on a 200 kV Osiris Transmission Electron Microscope.

CryoTEM samples were prepared on a Gatan Cryo Plunge III (Cp3). 3 μL of sample (at 1 mg/mL) was dropped on a lacey copper grid coated with a continuous carbon film. The Cp3 blotter was used to remove excess sample without damaging the carbon layer prior to plunge freezing. The frozen grid was mounted on a Gatan 626 single tilt cryo-holder and a transfer workstation with liquid nitrogen was used to maintain the specimen and holder under frozen conditions prior to imaging. The sample was imaged on a JEOL 2100 FEG. The microscope was operated at 200 kV. All images were recorded on a Gatan UltraScan CCD camera.

Red blood haemolysis assay.

De-identified human whole blood was acquired from Vanderbilt Technologies for Advanced Genomics (VANTAGE). Erythrocytes were pelleted at 500 rcf and washed three times with PBS. Following the third wash, erythrocytes were suspended in 100 mM PBS of desired pH and plated in a 96 well V-bottom plate. Erythrocytes were treated with nanoparticles at a concentration of 10 μg/mL at 37°C for one hour. Plates were then centrifuged at 700 rcf, and the supernatant was transferred to a 96 well flat bottom plate for quantification of hemoglobin leakage via absorbance spectroscopy (λ = 575 nm).

Cell Culture.

DC2.4 cells were kindly provided by Prof. Kenneth Rock (University of Massachusetts Medical School) and cultured in RPMI 1640 (Gibco) supplemented with 10% fetal bovine serum (Gibco), 100 U/mL penicillin (Gibco), 100 μg/mL streptomycin (Gibco), 2 mM L-glutamine, 50 μM 2-mercaptoethanol (Gibco), 1x nonessential amino acids (Cellgro), and 10 mM HEPES (Invitrogen). B16-Blue ISG, THP-1-Blue ISG, and RAW-Blue ISG cells were purchased from Invivogen, and cultured according to manufacturer specifications. No authentication of the cell lines were performed by the authors. All cells lines were tested for mycoplasma contamination and grown in a humidified atmosphere with 5% CO_2 at 37°C.

In vitro evaluation of CDN activity and cellular uptake.

THP-1 ISG, DC2.4, B16 ISG and RAW Blue ISG cell lines were plated at a density of 10,000, 10,000, 50,000, and 50,000 cells/well, respectively, in a 96 well plate. Cells were treated with indicated formulations for 24 hours. For ISG reporter cell lines, the relative expression of IFN-stimulated response element (ISRE) genes was examined using the QUANTI-Blue reagent (Invivogen). For dendritic cells, secreted IFN-β was quantified with the LumiKine™ Xpress mIFN-β ELISA kit (Invivogen).

To quantify relative cellular CDN uptake, B16.F10, RAW264.7, DC2.4, and primary murine NK cells were seeded at 100,000 cells/well in 12 well plates and treated with co-formulations of cdGMP-Dy547 (Axxora) and cGAMP for 2 hrs at concentrations of 2 ng/mL and 100 ng/mL, respectively. NK cells were isolated from spleens of 6–8 week old female C57BL6/J mice. Spleens were mechanically dissociated, strained through a 40 μm cell strainer, and enriched for NK cells through an EasySep™ mouse NK cell isolation kit (STEMCELL Technologies). After incubation for 2 hours, cells were suspended in a 2% BSA in PBS solution and analyzed *via* flow cytometry using a 561 nm excitation laser and 582/15 filter configuration on a BD LSRFortessa™.

Mouse Care and Experimentation.

Female C57BL/6 mice (6–8 weeks old) were purchased from The Jackson Laboratory (Bar Harbor, ME). All animals were maintained at the animal facilities of Vanderbilt University under specific pathogen-free conditions and treated in accordance with the regulations and guidelines of the Institutional Animal Care and Use Committee (IACUC). All animal experiments were approved by the Vanderbilt University IACUC.

IVIS Imaging.

B16.F10 melanoma cells were transduced to express luciferase in an ISRE-dependent manner via the Cignal Lenti Reporter construct (Qiagen). Transduced cells were grown and expanded in medium containing the selection agent puromycin at a concentration of 10 μg/mL. Transduction was verified by treating cells with mouse IFN-β and monitoring luciferase production.

5×10^4 B16.F10 cells containing the reporter construct were injected subcutaneously into the flank of 6–8 week old female C57BL/6 (Jackson Labs). Upon reaching ~100 mm^3, tumours were injected intratumourally with 100 μL PBS containing 10 μg of cGAMP in the appropriate formulation. Mice were injected intraperitoneally with 200 μL of 15mg/mL D-luciferin (ThermoFisher) in PBS. 15 minutes following injection, luminescence was quantified on the IVIS Lumina III (PerkinElmer) using Living Image software (version 4.5).

Gene Expression Analysis Following Intratumoural Administration.

Female C57BL6/J mice aged 6–8 weeks old were inoculated subcutaneously with 50,000 B16.F10 cells. Upon reaching an average size of ~100 mm^3, tumours were treated *via* intratumoural injection with 100 μL of either PBS, free cGAMP, or STING-NP nanoparticle formulations (10 μg cGAMP per injection). For qPCR analysis, tumours were harvested after four hours, and lysed in RLT lysis buffer (Qiagen) supplemented with 2% β-mercaptoethanol (Sigma) in a gentleMACS M tube with mechanical disruption using an OctoMACS tissue dissociator (Miltenyi). Tumour RNA was isolated with an RNeasy RNA isolation kit (Qiagen) with the RNAse free DNAse Set (Qiagen), used according to manufacturer specifications. cDNA was synthesized with the Bio-Rad iScript cDNA kit and analyzed *via* qPCR using the appropriate TaqMan kits (Thermo Fisher Scientific). TaqMan™ gene expression kits: Mouse Tnf: Mm00443258_m1. Mouse Ifnb1: Mm00439552_s1. Mouse Cxcl9: Mm00434946_m1. Mouse Cxcl10: Mm00445235_m1. Mouse Hmbs: Mm01143545_m1.

Quantification of CDN accumulation and *Ifnb1* expression in the tumour draining lymph node.

Subcutaneous B16.F10 tumours of ~100 mm^3 were injected with coformulations of cGAMP (10 μg) and cdGMP-Dy547 (0.2 μg). 1 hr after injection, the mice were sacrificed and the inguinal tumour draining lymph node was harvested, placed in RLT tissue lysis buffer (Qiagen), and homogenized using an OctoMACs tissue dissociator. cdGMP-Dy547 was quantified in the resulting lysate on a Synergy H1 plate reader (576/550 Ex/Em). Background fluorescence was removed by subtracting baseline fluorescence values of TDLN lysates from PBS treated tumour bearing mice. For quantification of *Ifnb1* expression, subcutaneous B16.F10 tumours were injected with cGAMP formulations (10 μg). TDLNs were harvested 2 hrs after injection. mRNA isolation, cDNA synthesis, and qPCR quantification of *Ifnb1* transcription were performed as described above.

NanoString nCounter Analysis.

100 ng of RNA was isolated as previously described from tumour samples 4h after treatment and analyzed by nanoString nCounter gene expression analysis using the PanCancer

Immune Profiling Panel. Fold change was calculated by comparing against average normalized gene expression values of PBS treated tumours. All statistical significance and clustering analysis was performed in R (http://cran.r-project.org).

Flow Cytometric Analysis of the B16.F10 Tumour Microenvironment.

B16.F10 tumours were established subcutaneously in C57BL6/J mice as previously described and treated intratumourally with either PBS or coformulations of cGAMP (10 μg) and cdGMP-Dy547 (0.2 μg). 48 hours after treatment, tumours and the inguinal draining lymph node were harvested, mechanically dissociated with an OctoMACs separator, and digested in a solution of 125 μg/mL DNAse I (Worthington) and 500μg/mL Collagenase III (Worthington) in RPMI 1640 media for 30 minutes at 37˚C. Tumours and lymph nodes were strained through a 40 μm cell strainer and treated with ACK Lysing Buffer (Gibco). Cells were diluted to a concentration of 2×10^7 cells/mL in PBS containing 2% BSA for FACS staining. 100 μL of cell suspension for each flow test was transferred into a 96 well plate and treated with FcX (Biolegend) according to manufacturer specifications. Samples were stained with several panels of the antibodies BV650-αCD45 (30– 19 F11), PE/Cy5-αCD11b (M1/70), PE-αCD11c (N418), PE/Cy7-αNK1.1 (PK136), APC/Cy7– 20 αF4/80 (BM8), APC/Cy7-αMHC-II (10.3.6), PE-αCD206 (C068C2), APC-αCD86 (GL-1), APC-αCD3 (17A2), APC/Cy7αCD4 (RM4–5), and PE/Cy5-αCD8α (53.6.7) (Biolegend). Cells were washed twice, suspended in PBS containing 2% FBS and 200 nM DAPI before analysis on a BD LSRFortessa or BD LSR II flow cytometer (Supplementary Figure S14).

For intracellular cytokine analysis, 10^6 cells were seeded in a 6 well plate in DMEM containing 10% FBS and supplemented with PMA/Ionomycin/Brefeldin A cocktail (Biolegend) according to manufacturer specification. After 4h, cells were washed, stained with antibodies against CD3, CD4, and CD8α, fixed with fixation buffer (Biolegend) and subsequently stained intracellularly with antibodies against TNF-α (MP6-XT22), IFN-γ (XMG1.2), IL-4 (11B11), and IL-10 (JES5–16E3) (Biolegend) in Intracellular Staining Permeabilization Wash Buffer (Biolegend). All flow cytometry data were analyzed using FlowJo software (version 10; Tree Star, Inc.).

Treatment of B16.F10 subcutaneous tumours.

5×10^4 B16.F10 cells were injected subcutaneously into the flank of 6–8 year old mice in 100 μL of serum free RPMI 1640 media. Tumour volume was measured every other day via caliper measurements, and tumour volume calculated using the equation $V = \frac{1}{2} \times L \times W \times H$. Upon reaching sizes of ~100 mm^3, tumours were treated intratumourally with 100 μL of PBS containing 10 μg of 2’3’-cGAMP in various formulations. Mice were sacrificed upon tumour burden endpoint of 1500 mm^3. For single tumour models, upon reaching a tumour volume of ~100 mm^3, tumours were injected intratumourally with 100 μL of the appropriate formulation in pH 7.4 PBS. Mice were injected 3x with treatments spaced 4 days apart. For contralateral studies, mice were inoculated on each flank subcutaneously. When the larger of the two tumours reached ~100 mm^3, it was injected with 100 uL of the appropriate formulation and designated as the primary tumour, with the untreated tumour designated as the contralateral tumour. For mice treated with checkpoint blockade, mice were injected

intraperitoneally with 100 uL of PBS containing 100 μg of both anti-PD1 (RMP1–14, BioXCell), and anti-CTLA4 (9D9, BioXCell). Treatments were spaced 4 days apart. For evaluation via systemic administration, mice were injected in the caudal vein with 100 uL of PBS containing the appropriate formulation seven days following a tumour inoculum of 5×10^5 B16.F10 cells (average volume = 30 mm^3). Treatments were spaced 4 days apart.

Analysis of blood chemistry and hepatocellular toxicity.

Upon reaching the tumour size endpoint, blood was harvested *via* submandibular bleeding, allowed to clot and used to prepare serum by centrifugation at 4000xg. Serum was tested by the Vanderbilt Translational Pathology Shared Resource (TPSR) for levels of alanine aminotransferase, bilirubin, and creatinine. Livers were harvested, fixed in a 10% formalin in PBS solution, paraffin embedded, and sectioned into 5 μm sections for H&E staining. Interpretation was completed by a board-certified veterinary pathologist under masked conditions.

Ex vivo stimulation of resected human metastatic melanoma.

All experiments using human samples were performed in compliance with United States Federal Policy for the Protection of Human Subjects and guidelines set forth by the Vanderbilt University Human Research Protections Program. Experiments were approved by the Vanderbilt University Institutional Review Board, and all patients were consented for research use of biospecimens (Vanderbilt University Medical Center IRB # 030220). Within an hour of surgical resection at Vanderbilt University Medical Center, human melanoma tumours were submerged in DMEM/F12 media (Gibco) supplemented with 10% FBS and divided into 9 sections using a scalpel. Individual sections were then placed in a 12 well plate containing 1 mL of media and injected with STING-NP, free cGAMP, or PBS with a syringe, reaching a final concentration of 100 ng/mL of cGAMP within each well. 24 hours after treatment, RNA isolation, cDNA synthesis, and qPCR analysis were then performed as described previously. TaqMan™ gene expression kits: Human Tnf: Hs00174128_m1. Human Ifnb1: Hs01077958_s1. Human Cxcl10: Hs00171042_m1. Human Hmbs: Hs00609296_g1.

Supplementary Material

Refer to Web version on PubMed Central for supplementary material.

Acknowledgments

We gratefully acknowledge Kenneth Rock for providing DC2.4 cells, Craig Duvall for use of gel permeation chromatography equipment and IVIS imaging system, Ann Richmond and Anna Vilgelm for consultation on flow cytometry protocols, and Julie Rhoades and Alyssa Merkel for technical advice on tumor models. We thank the Koch Institute Swanson Biotechnology Center, specifically the Nanotechnology Materials Core Facility, for technical support on cryoEM, the core facilities of the Vanderbilt Institute of Nanoscale Sciences and Engineering (VINSE) for use of dynamic light scattering and TEM instruments, the VUMC Flow Cytometry Shared Resource, supported by the Vanderbilt Ingram Cancer Center (P30 CA68485) and the Vanderbilt Digestive Disease Research Center (DK058404), for the usage of BD 3-laser LSRII flow cytometery, the Vanderbilt Translational Pathology Shared Resource (supported in part by the NCI/NIH Cancer Center Support Grant 5P30 CA684850–19), and the Vanderbilt Technologies for Advanced Genomics (VANTAGE). 2’3’-cGAMP was provided by the Vanderbilt Institute of Chemical Biology Chemical Synthesis Core. This research was supported by grants from the National Science Foundation CBET-1554623 (JTW), Alex’s Lemonade Stand Foundation SID924 (JTW), the National Institutes of Health K23 CA204726/CA/NCI (DBJ), R00CA181491 (JMB), 5R35GM119569–03 (MA), the

Vanderbilt-Ingram Cancer Center Support Grant P30 CA68485, Vanderbilt Ingram Cancer Center (VICC) Ambassador Discovery Grant (MA), VICC-Vanderbilt Center for Immunobiology Pilot Grant (JTW), the Melanoma Research Alliance 503565 (JTW), and also supported by a Stand Up To Cancer Innovative Research Grant, Grant Number SU2C-AACR-IRG 20–17 (JTW). Stand Up To Cancer (SU2C) is a program of the Entertainment Industry Foundation. Research grants are administered by the American Association for Cancer Research, the scientific partner of SU2C.

References

1. Ribas A & Wolchok JD Cancer immunotherapy using checkpoint blockade. Science 359, 1350–1355 (2018). [PubMed: 29567705]
2. Sharma P & Allison JP The future of immune checkpoint therapy. Science 348, 56–61 (2015). [PubMed: 25838373]
3. Vanpouille-Box C et al. Trial watch: Immune checkpoint blockers for cancer therapy. Oncoimmunology 6, e1373237 (2017). [PubMed: 29147629]
4. Khalil DN, Smith EL, Brentjens RJ & Wolchok JD The future of cancer treatment: immunomodulation, CARs and combination immunotherapy. Nat Rev Clin Oncol 13, 394 (2016). [PubMed: 27118494]
5. Gotwals P et al. Prospects for combining targeted and conventional cancer therapy with immunotherapy. Nat Rev Cancer 17, 286–301 (2017). [PubMed: 28338065]
6. Binnewies M et al. Understanding the tumor immune microenvironment (TIME) for effective therapy. Nat Med 24, 541–550 (2018). [PubMed: 29686425]
7. Chen DS & Mellman I Elements of cancer immunity and the cancer-immune set point. Nature 541, 321–330 (2017). [PubMed: 28102259]
8. Fridman WH, Zitvogel L, Sautes-Fridman C & Kroemer G The immune contexture in cancer prognosis and treatment. Nat Rev Clin Oncol 14, 717–734 (2017). [PubMed: 28741618]
9. Woo SR et al. STING-dependent cytosolic DNA sensing mediates innate immune recognition of immunogenic tumors. Immunity 41, 830–842 (2014). [PubMed: 25517615]
10. Deng L et al. STING-dependent cytosolic DNA sensing promotes radiation-induced type I interferon-dependent antitumor immunity in immunogenic tumors. Immunity 41, 843–852 (2014). [PubMed: 25517616]
11. Gao P et al. Cyclic [G(2’,5’)pA(3’,5’)p] is the metazoan second messenger produced by DNA-activated cyclic GMP-AMP synthase. Cell 153, 1094–1107 (2013). [PubMed: 23647843]
12. Diner EJ et al. The innate immune DNA sensor cGAS produces a noncanonical cyclic dinucleotide that activates human STING. Cell Rep 3, 1355–1361 (2013). [PubMed: 23707065]
13. Ablasser A et al. cGAS produces a 2’−5’-linked cyclic dinucleotide second messenger that activates STING. Nature 498, 380–384 (2013). [PubMed: 23722158]
14. Zhang X et al. Cyclic GMP-AMP containing mixed phosphodiester linkages is an endogenous high-affinity ligand for STING. Mol Cell 51, 226–235 (2013). [PubMed: 23747010]
15. Gao P et al. Structure-function analysis of STING activation by c[G(2’,5’)pA(3’,5’)p] and targeting by antiviral DMXAA. Cell 154, 748–762 (2013). [PubMed: 23910378]
16. Chen Q, Sun L & Chen ZJ Regulation and function of the cGAS-STING pathway of cytosolic DNA sensing. Nat Immunol 17, 1142–1149 (2016). [PubMed: 27648547]
17. Corrales L, McWhirter SM, Dubensky TW, Jr. & Gajewski TF The host STING pathway at the interface of cancer and immunity. J Clin Invest 126, 2404–2411 (2016). [PubMed: 27367184]
18. Wang H et al. cGAS is essential for the antitumor effect of immune checkpoint blockade. Proc Natl Acad Sci U S A 114, 1637–1642 (2017). [PubMed: 28137885]
19. Ishikawa H, Ma Z & Barber GN STING regulates intracellular DNA-mediated, type I interferon-dependent innate immunity. Nature 461, 788–792 (2009). [PubMed: 19776740]
20. Corrales L et al. Direct activation of STING in the tumor microenvironment leads to potent and systemic tumor regression and immunity. Cell Rep 11, 1018–1030 (2015). [PubMed: 25959818]
21. Demaria O et al. STING activation of tumor endothelial cells initiates spontaneous and therapeutic antitumor immunity. PNAS 112, 15408–15413 (2015). [PubMed: 26607445]

22. Ohkuri T et al. Intratumoral administration of cGAMP transiently accumulates potent macrophages for anti-tumor immunity at a mouse tumor site. Cancer Immunol Immunother 66, 705–716 (2017). [PubMed: 28243692]
23. Curran E et al. STING pathway activation stimulates potent immunity against acute myeloid leukemia. Cell Rep 15, 2357–2366 (2016). [PubMed: 27264175]
24. Fu J et al. STING agonist formulated cancer vaccines can cure established tumors resistant to PD-1 blockade. Sci Transl Med 7, 283ra252 (2015).
25. Dubensky TW, Jr., Kanne DB & Leong ML Rationale, progress and development of vaccines utilizing STING-activating cyclic dinucleotide adjuvants. Ther Adv Vaccines 1, 131–143 (2013). [PubMed: 24757520]
26. Koshy ST, Cheung AS, Gu L, Graveline AR & Mooney DJ Liposomal delivery enhances immune activation by STING agonists for cancer immunotherapy. Advanced Biosystems 1, 1600013 (2017). [PubMed: 30258983]
27. Hanson MC et al. Nanoparticulate STING agonists are potent lymph node-targeted vaccine adjuvants. The Journal of Clinical Investigation 125, 2532–2546 (2015). [PubMed: 25938786]
28. Mullard A Can innate immune system targets turn up the heat on ‘cold’ tumours? Nat Rev Drug Discov 17, 3–5 (2018). [PubMed: 29282375]
29. Vrignaud S, Benoit JP & Saulnier P Strategies for the nanoencapsulation of hydrophilic molecules in polymer-based nanoparticles. Biomaterials 32, 8593–8604 (2011). [PubMed: 21831421]
30. Manganiello MJ, Cheng C, Convertine AJ, Bryers JD & Stayton PS Diblock copolymers with tunable pH transitions for gene delivery. Biomaterials 33, 2301–2309 (2012). [PubMed: 22169826]
31. Wilson JT et al. Enhancement of MHC-I antigen presentation via architectural control of pH-responsive, endosomolytic polymer nanoparticles. The AAPS Journal 17, 358–369 (2014). [PubMed: 25501498]
32. O’Neil CP, Suzuki T, Demurtas D, Finka A & Hubbell JA A novel method for the encapsulation of biomolecules into polymersomes via direct hydration. Langmuir 25, 9025–9029 (2009). [PubMed: 19621886]
33. Kilchrist KV, Evans BC, Brophy CM & Duvall CL Mechanism of enhanced cellular uptake and cytosolic retention of MK2 inhibitory peptide nano-polyplexes. Cell Mol Bioeng 9, 368–381 (2016). [PubMed: 27818713]
34. Nelson CE et al. Balancing cationic and hydrophobic content of PEGylated siRNA polyplexes enhances endosome escape, stability, blood circulation time, and bioactivity in vivo. ACS Nano (2013).
35. Discher DE & Ahmed F Polymersomes. The Annual Review of Biomedical Engineering 8, 323–341 (2006).
36. Jain S & Bates FS Consequences of nonergodicity in aqueous binary PEO-PB micellar dispersions. Macromolecules 2004, 1511–1523 (2004).
37. Mai Y & Eisenberg A Self-assembly of block copolymers. Chem Soc Rev 41, 5969–5985 (2012). [PubMed: 22776960]
38. Parker BS, Rautela J & Hertzog PJ Antitumour actions of interferons: implications for cancer therapy. Nat Rev Cancer 16, 131–144 (2016). [PubMed: 26911188]
39. Yin H et al. Non-viral vectors for gene-based therapy. Nat Rev Genet 15, 541–555 (2014). [PubMed: 25022906]
40. Wilson DR et al. Biodegradable STING agonist nanoparticles for enhanced cancer immunotherapy. Nanomedicine 14, 237–246 (2018). [PubMed: 29127039]
41. Harlin H et al. Chemokine expression in melanoma metastases associated with CD8+ T-cell recruitment. Cancer Res 69, 3077–3085 (2009). [PubMed: 19293190]
42. Munn DH & Mellor AL The tumor-draining lymph node as an immune-privileged site. Immunological Reviews 213, 146–158 (2006). [PubMed: 16972902]
43. Reddy ST, Rehor A, Schmoekel HG, Hubbell JA & Swartz MA In vivo targeting of dendritic cells in lymph nodes with poly(propylene sulfide) nanoparticles. J Control Release 112, 26–34 (2006). [PubMed: 16529839]

44. Reddy ST et al. Exploiting lymphatic transport and complement activation in nanoparticle vaccines. Nat Biotechnol 25, 1159–1164 (2007). [PubMed: 17873867]
45. Lizotte PH et al. In situ vaccination with cowpea mosaic virus nanoparticles suppresses metastatic cancer. Nat Nanotechnol 11, 295–303 (2016). [PubMed: 26689376]
46. Mantovani A, Cassatella MA, Costantini C & Jaillon S Neutrophils in the activation and regulation of innate and adaptive immunity. Nat Rev Immunol 11, 519–531 (2011). [PubMed: 21785456]
47. Liang H et al. Host STING-dependent MDSC mobilization drives extrinsic radiation resistance. Nat Commun 8, 1736 (2017). [PubMed: 29170400]
48. Shi L et al. PD-1 blockade boosts radiofrequency ablation-elicited adaptive immune responses against tumor. Clin Cancer Res 22, 1173–1184 (2016). [PubMed: 26933175]
49. Ries CH et al. Targeting tumor-associated macrophages with anti-CSF-1R antibody reveals a strategy for cancer therapy. Cancer Cell 25, 846–859 (2014). [PubMed: 24898549]
50. Rudqvist NP et al. Radiotherapy and CTLA-4 blockade shape the TCR repertoire of tumor-infiltrating T cells. Cancer Immunol Res 6, 139–150 (2018). [PubMed: 29180535]
51. Murthy V, Minehart J & Sterman DH Local immunotherapy of cancer: Innovative approaches to harnessing tumor-specific immune responses. J Natl Cancer Inst 109 (2017).
52. Overwijk WW et al. Tumor regression and autoimmunity after reversal of a functionally tolerant state of self-reactive CD8+ T cells. J Exp Med 198, 569–580 (2003). [PubMed: 12925674]
53. Moynihan KD et al. Eradication of large established tumors in mice by combination immunotherapy that engages innate and adaptive immune responses. Nat Med 22, 1402–1410 (2016). [PubMed: 27775706]
54. Ghosh S, Basu S & Thayumanavan S Simultaneous and reversible functionalization of copolymers for biological applications. Macromolecules 2006, 5595–5597 (2006).
55. Matini T et al. Synthesis and characterization of variable conformation pH responsive block co-polymers for nucleic acid delivery and targeted cell entry. Polym. Chem 5, 1626–1636 (2014).
56. Gaffney BL, Veliath E, Zhao J & Jones RA One-flask synthesis of c-di-GMP and the [Rp,Rp] and [Rp,Sp] thiophosphate analogues. Organic Letters 12, 3269–3271 (2010). [PubMed: 20572672]

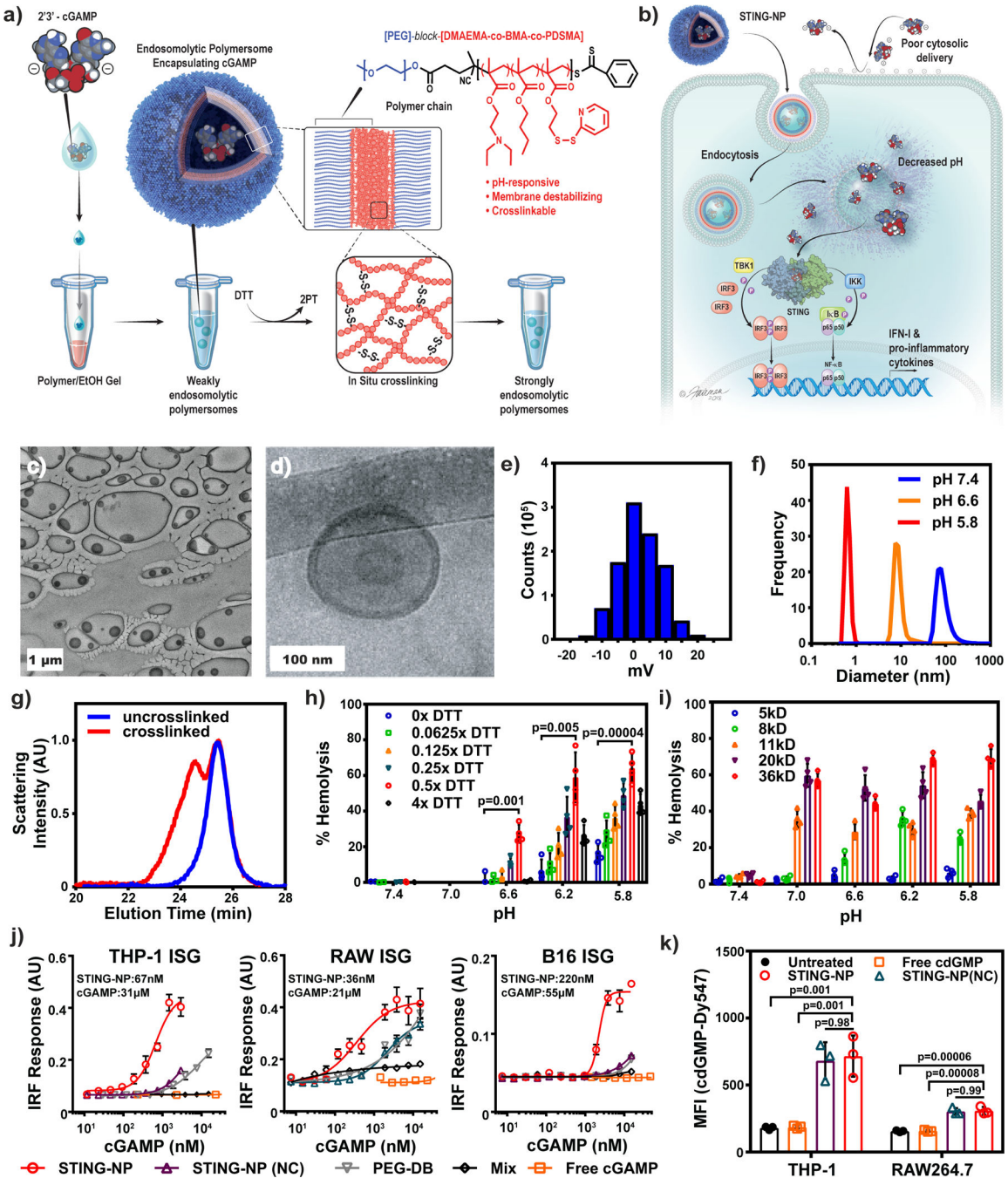

Figure 1 |. Design, optimization, and characterization of STING-NPs.

a) Schematic of STING-NP structure and mechanism of enhanced intracellular delivery of 2’3’-cGAMP. cGAMP is encapsulated in endosomolytic polymersomes assembled from pH-responsive diblock copolymers. After polymersome self-assembly and cGAMP loading, polymer chains are crosslinked *in situ* via partial reduction of PDS groups with DTT resulting in formulation of disulfide crosslinks. 2PT: 2-pyridinethione. **b)** STING-NPs enhance intracellular uptake of cGAMP and in response to decreased pH within endosomal compartments disassemble and promote endosomal escape of cGAMP to the cytosol.

Representative conventional **(c)** and cryo **(d)** transmission electron micrographs of polymersomes assembled using PEG_{2kDa}-$DBP_{4.5kDa}$ polymers. Cryo-EM was performed once, while conventional EM was repeated independently twice with similar results. **e)** Zeta potential distribution of polymersomes at pH 7.4. Repeated twice independently with similar results. **f)** Dynamic light scattering analysis of number average particle size distribution of STING-NPs at extracellular and endosomal pH. Repeated twice independently with similar results. **g)** Gel permeation chromatograms of PEG_{2kDa}-$DBP_{4.5kDa}$ copolymers before and after *in situ* crosslinking of polymersomes. Repeated twice independently with similar results. **h)** Effect of the degree of crosslinking, represented by equivalents of DTT to PDSMA, on pH-dependent membrane destabilizing activity as measured using an erythrocyte haemolysis assay (n=4 biologically independent samples, two-tailed Student's t-test). **i)** Effect of second block molecular weight (MW) in PEG_{2kDa}-DB_{MW} copolymers on pH-dependent haemolysis (n=4 biologically independent samples). **j)** Dose-response curves of type-I IFN (IFN-I) response elicited by indicated cGAMP-containing formulations in THP-1, RAW264.7, and B16 interferon stimulated genes (ISG) cells with an IFN regulatory factor (IRF)-inducible reporter construct. STING-NP(NC): non-crosslinked; PEG-DB: cGAMP delivered with polymersomes assembled using non-crosslinkable PEG_{2kDa}-DB_{5kDa} chains; Mix: physical mixture of empty crosslinked PEG_{2kDa}-*b*-$DBP_{4.5kDa}$ polymersomes and free cGAMP (n=4 biologically independent samples). **k)** Flow cytometric quantification of uptake of cdGMP-Dy547 co-delivered with cGAMP in indicated formulation by THP-1 and RAW264.7 cells (n=3 biologically independent samples, one-way ANOVA with Tukey test). All statistical data are presented as mean ± SD.

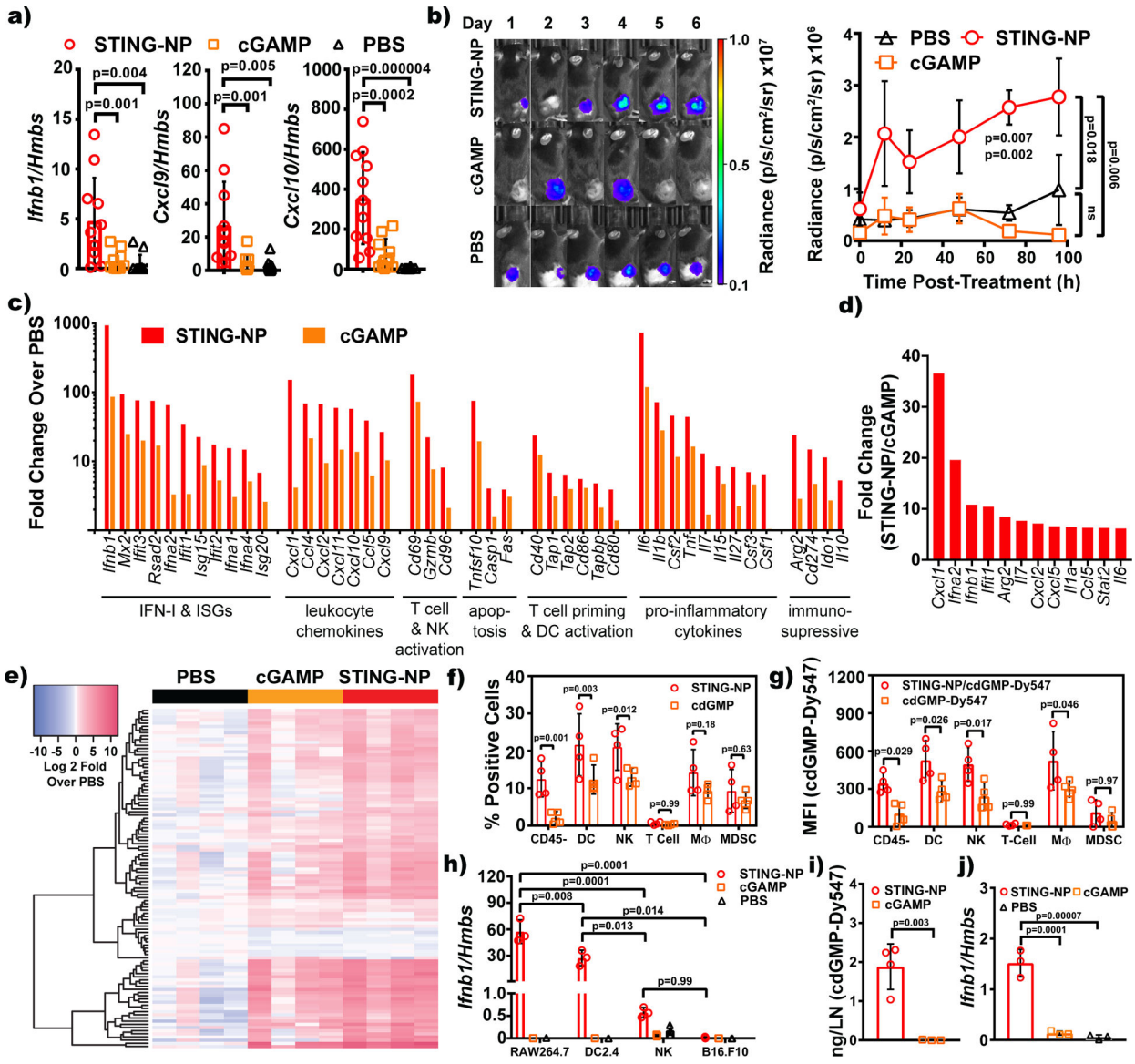

Figure 2 |. STING-NPs enhance the delivery and immunostimulatory activity of cGAMP in the tumour microenvironment.

a) qPCR analysis of *Ifnb1*, *Cxcl9*, and *Cxcl10* expression in B16.F10 tumours 4h after intratumoural administration of STING-NP, free cGAMP, or PBS as vehicle control (for STING-NP, cGAMP and PBS, respectively, n=11, 10, and 12 biologically independent samples, one-way ANOVA with Tukey test) at a dose corresponding to 10 μg cGAMP. **b)** Luminescence of SC B16.F10 tumours expressing an ISRE luciferase reporter following intratumoural treatment with cGAMP formulations (mean ± SEM; for STING-NP, cGAMP and PBS, n=5, 4, and 5 biologically independent samples, two-way ANOVA with Tukey test). The values p=0.007 and p=0.002 denotes significance between STING-NP and PBS and cGAMP, respectively, at t=72h; p=0.018: STING-NP vs. PBS at 96h; p=0.006: STING-NP vs. cGAMP at 96h. **c)** Summary of selected differentially expressed genes (p <0.05, one-way ANOVA) in response to treatment with STING-NPs or cGAMP (n=4 biologically independent samples). **d)** Ranked analysis of differential gene expression between STING-

NP and cGAMP administration (n=4 biologically independent samples). **e)** Unsupervised hierarchical clustering of relative gene expression. **f)** Percentage of cdGMP-Dy547^{+} cells amongst cell populations in the TME following intratumoural administration of Dy547-cdGMP formulations (n=4 biologically independent samples, one-way ANOVA with Tukey test). **g)** Flow cytometric quantification of the median fluorescent intensity (MFI) of cdGMP-Dy547^{+} cells among indicated cell populations in the TME (n=4 biologically independent samples, two-way ANOVA with Sidak's multiple comparison test). **h)** *Ifnb1* expression following *in vitro* incubation with STING-NP, cGAMP, or PBS for 4h at doses equivalent to 150 nM cGAMP in RAW264.7 macrophages, DC2.4 dendritic cells, primary NK cells, and B16.F10 melanoma cells (n=3 biologically independent samples, one-way ANOVA with Tukey test). Significance levels are shown for comparisons between cells treated with STING-NP formulations. **i)** Fluorescence spectrophotometric quantification of cdGMP-dy547 accumulation in the sentinel LN 2h following intratumoural administration (for cGAMP and STING-NP, respectively, n=3,4 biologically independent samples, two-tailed Student's t-test). **j)** *Ifnb1* expression in the sentinel (inguinal) LN following 4h following intratumoural administration (n=3 biologically independent samples, one-way ANOVA with Tukey test). Unless otherwise noted, statistical data are presented as mean ± SD.

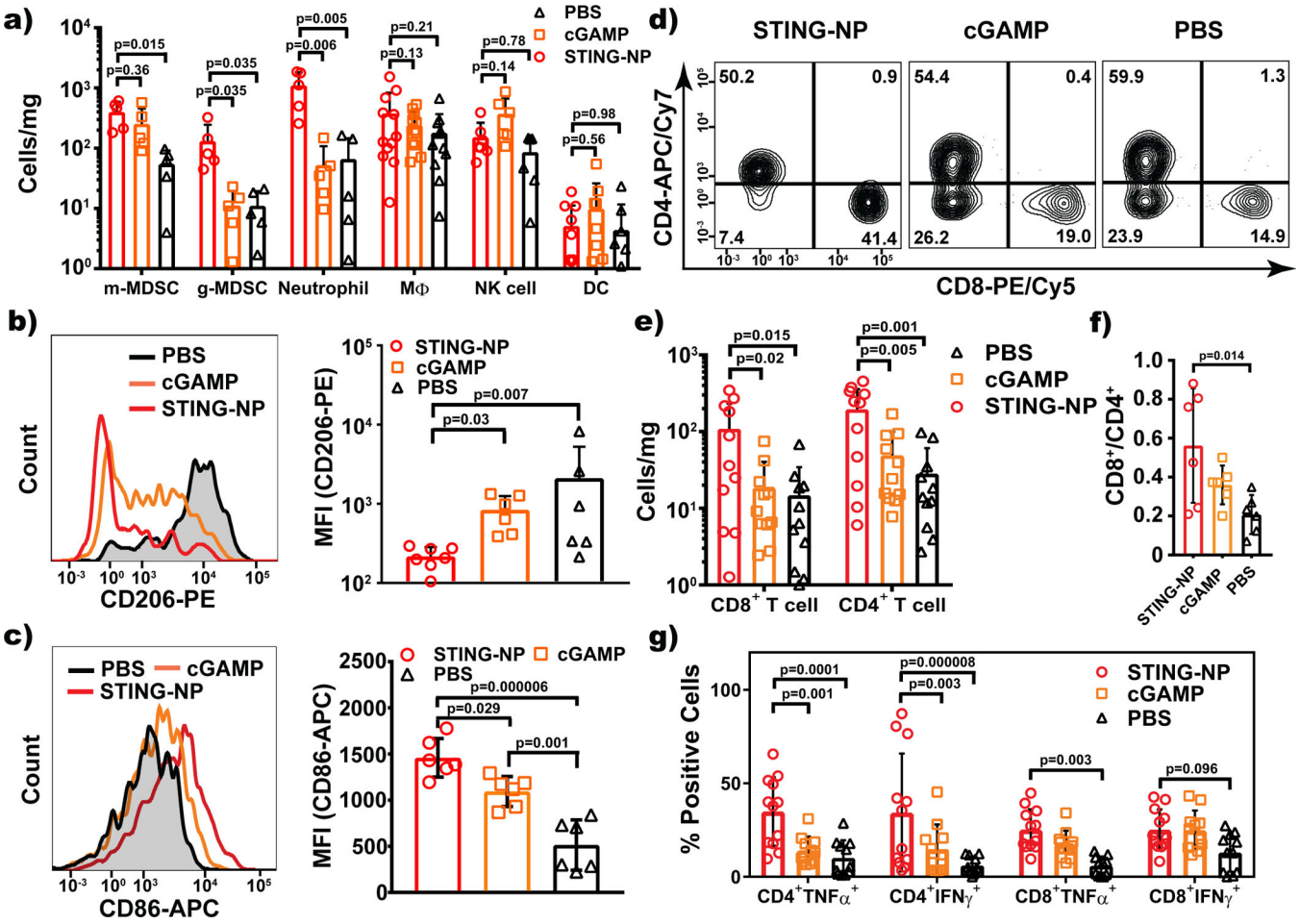

Figure 3 |. STING-NPs shift the immunocellular composition of the tumor microenvironment.

a) Flow cytometric quantification of the number of monocytic ($CD11b^+Ly6c^+Ly6g^-$) and granulocytic ($CD11b^+Ly6c^+Ly6g^+SSC^{hi}$) myeloid derived suppressor cells, activated neutrophils ($CD11b^+Ly6c^+Ly6g^+SSC^{lo}$), macrophages (mϕ; $CD11b^+F4/80^+$), natural kill (NK) cells ($NK1.1^+$), and dendritic cells (DC; $CD11c^+$MHC-II^+) 48h following intratumoural injection (for m-MDSC, g-MDSC, neutrophil, macrophage, NK cells, and DCs, respectively n=6, 6, 6, 11, 11, and 11 biologically independent samples, one-way ANOVA with Tukey test). **b)** Representative flow cytometry histogram (left) and quantification (right) of CD86 expression by dendritic cells in the inguinal lymph node (n=6 biologically independent samples, one-way ANOVA with Tukey test). **c)** Representative flow cytometry histogram (left) and quantification (right) of CD206 expression by intratumoral macrophages (n=6 biologically independent samples, Kruskal-Wallace test with Dunn's multiple comparison test) **d)** Representative flow cytometry dot plot and **e)** quantification of tumour infiltrating $CD4^+$ and $CD8^+$ T cells 48h following intratumoural injection (n=11 biologically independent samples, one-way ANOVA with Tukey test). **f)** Ratio of $CD8^+$ to $CD4^+$ T cells in the TME (n=11 biologically independent samples, one-way ANOVA with Tukey test). **g)** Intracellular cytokine staining and flow cytometry was used to evaluate TNF-α and IFN-γ production by tumour infiltrating $CD4^+$ and $CD8^+$ T cells in response to PMA/ionomycin stimulation (n=11 biologically independent samples,

two-way ANOVA with Tukey test). Statistical data are represented as mean ± SD. All experiments were repeated once independently with similar results.

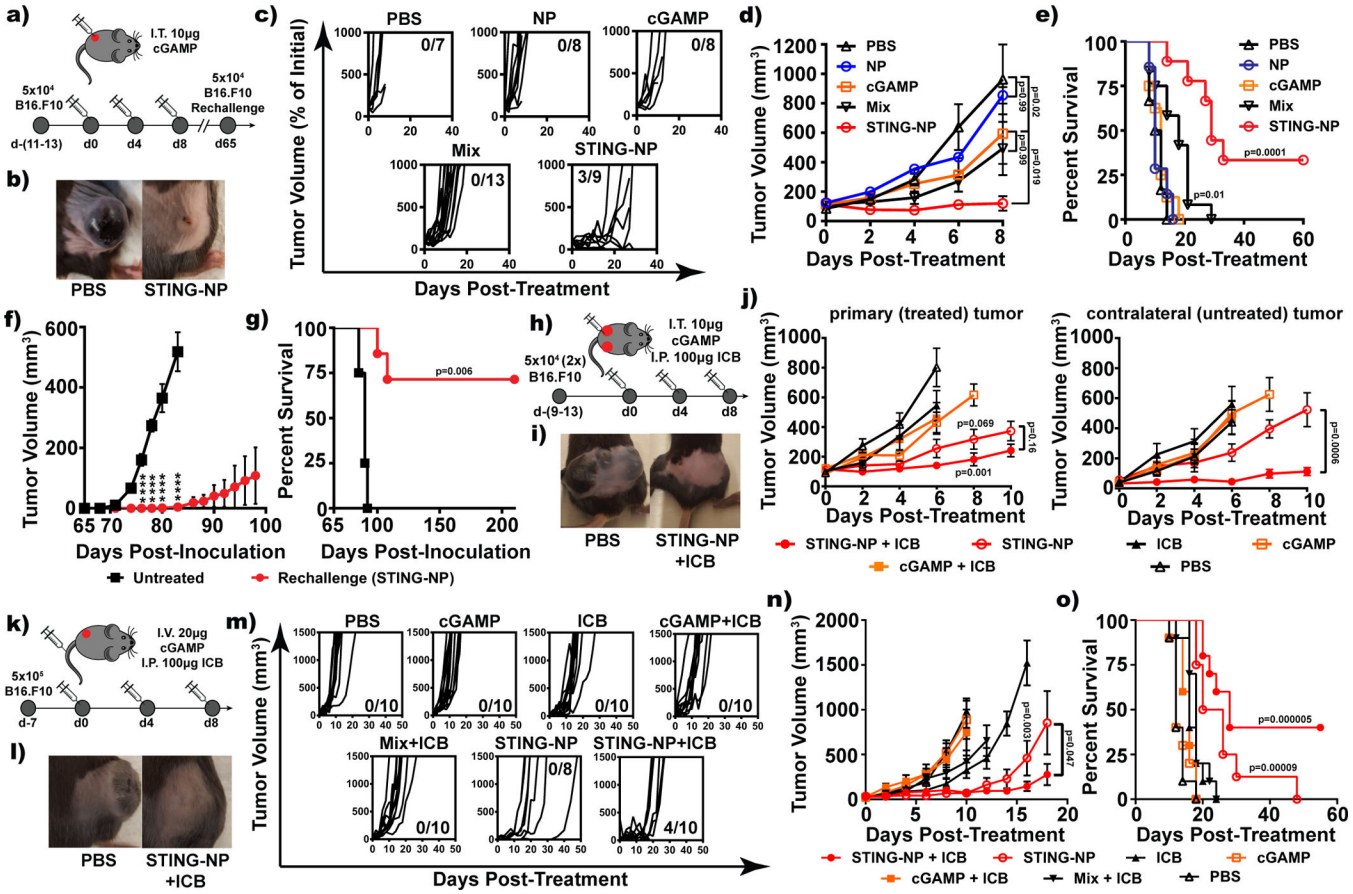

Figure 4 |. STING-NPs enhance the immunotherapeutic efficacy of cGAMP and synergize with immune checkpoint blockade.

a) Intratumoural administration and tumour rechallenge scheme for mice with a single established B16.F10 tumour. Mice with 100 mm^3 subcutaneous (SC) tumours were administered STING-NPs, free cGAMP, empty nanoparticles (NP), a physical mixture of empty NPs and cGAMP (Mix), or PBS intratumourally (I.T.). **b)** Photographs of tumours 8 days after treatment. Repeated twice independently with similar results. **c)** Spider plots of individual tumour growth curves with number of complete responses (CRs) denoted. Repeated twice independently with similar results. **(d)** Mean tumour volume from 3 independent experiments (for PBS, NP, cGAMP, Mix, and STING-NP, n=7, 8, 8, 13, and 9 biologically independent samples; Kruskal-Wallis test with Dunn's multiple comparisons test). **(e)** Kaplan-Meier survival curves of mice treated with indicated formulation using 1500 mm^3 tumour volume as endpoint criteria (for PBS, NP, cGAMP, Mix, and STING-NP, n=7, 8, 8, 13, and 9 biologically independent samples, two-tailed Mantel-Cox test). **f)** Mice demonstrating complete responses to STING-NP treatment were rechallenged with B16.F10 cells on the contralateral flank 65 days after inoculation without any further treatment. (For treatment naïve and rechallenged CRs, n=4 and 7 biologically independent samples. ****: $p<0.0001$, two-tailed Student t test). **g)** Kaplan-Meier survival curves for treatment naïve and STING-NP treated CRs (n=7, two-tailed Mantel-Cox test). **h)** Treatment scheme for mice with two concurrently established contralateral B16.F10 tumours. Mice were treated with cGAMP containing formulations intratumourally in one tumour and administered a

combination of anti-PD1 and anti-CTLA-4 antibodies (ICB) intraperitoneally (I.P.) three times, 4 days apart. **i)** Representative images of tumours 8 days after initiation of STING-NP or PBS administration (injected into left flank tumour). Repeated independently once with similar results. **j)** Average tumour volume of injected primary and untreated contralateral tumour (for PBS, cGAMP, ICB, cGAMP+ICB, STING-NP, and STING-NP+ICB, n=11, 7, 6, 10, 10, and 12 biologically independent samples, two-tailed Mann-Whitney test); p=0.069, p=0.001 denotes significance levels of STING-NP and STING-NP + ICB treated mice, respectively, vs. those treated with ICB alone. Kruskal-Wallis test with Dunn's multiple comparison test. **k)** Treatment scheme for mice treated intravenously (I.V.) with cGAMP formulations and I.P. with ICB 3 times, 4 days apart. **l)** Representative images of tumours 8 days after initiation of treatment. Repeated twice independently with similar results. **m)** Spider plots of individual tumour growth curves of intravenously treated mice, **n)** average tumour volume (two-tailed Mann-Whitney test, p=0.003 denotes significance of STING-NP relative to mix+ICB group), and **o)** Kaplan-Meier survival analysis (two-tailed Mantel-Cox test). **m-o**: for PBS, cGAMP, ICB, cGAMP+ICB, Mix+ICB, STING-NP, and STING-NP+ICB, n= 10, 10, 10, 10, 10, 8, and 10 biologically independent samples. All statistical data are represented as mean ± SEM.

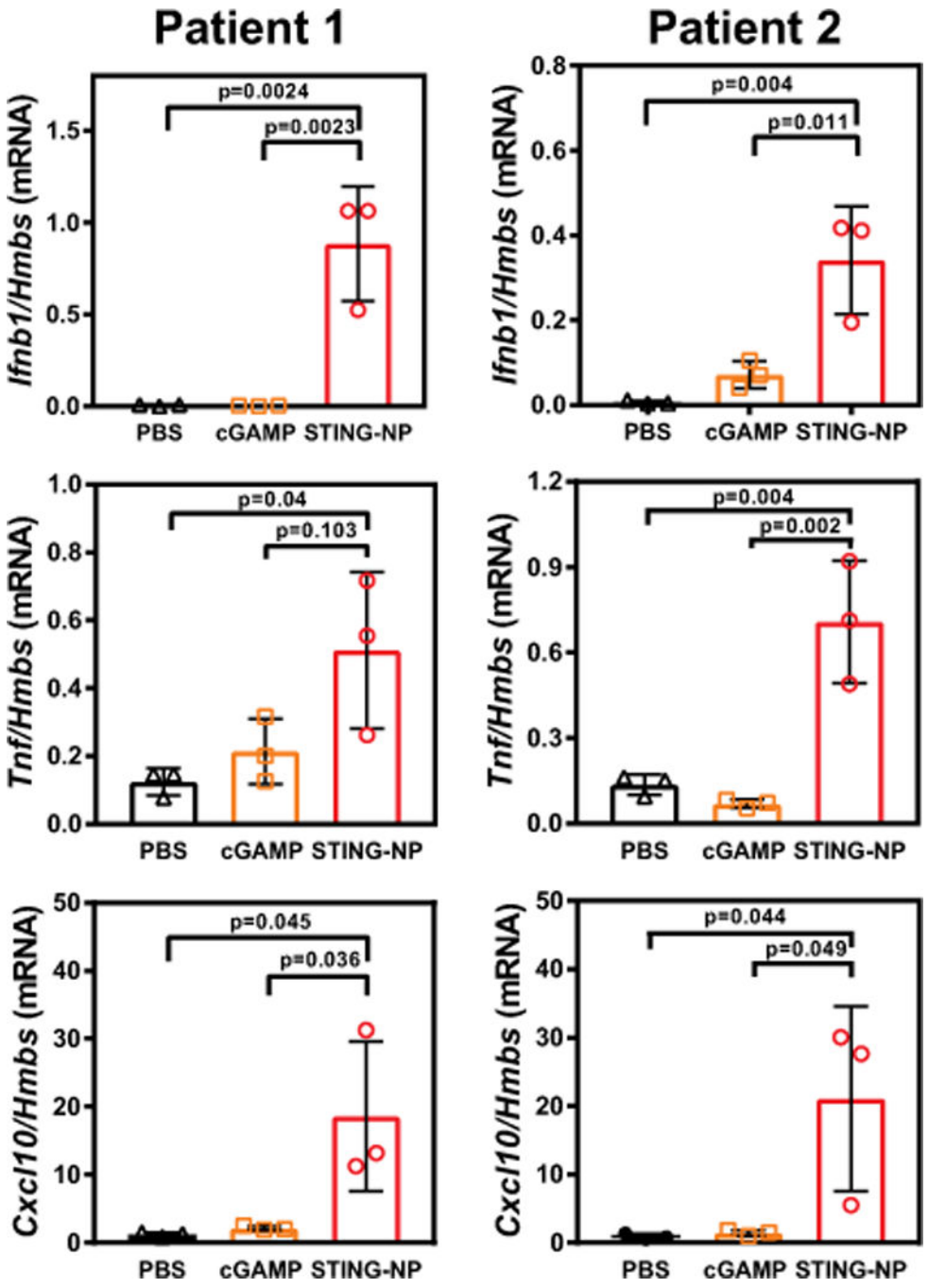

Figure 5 |. STING-NPs enhance cGAMP activity in human metastatic melanoma.

Surgically resected melanoma metastases were divided into nine sections (3 per treatment, one-way ANOVA with Tukey test), randomized, and injected intratumourally with STING-NPs or cGAMP at 150 nM and cultured for 24 h. qPCR analysis of *Ifnb1*, *Tnf* and *Cxcl10* gene expression in tissue freshly isolated from two different melanoma patients after indicated treatment. All statistical data are presented as mean ± SD.